



# Cavity QED based on room temperature atoms interacting with a photonic crystal cavity: a feasibility study

Hadiseh Alaeian<sup>1,2</sup> · Ralf Ritter<sup>1,2</sup> · Muamera Basic<sup>1,2</sup> · Robert Löw<sup>1,2</sup> · Tilman Pfau<sup>1,2</sup>

Received: 31 May 2019 / Accepted: 9 December 2019 / Published online: 16 January 2020  
© The Author(s) 2020

## Abstract

The paradigm of cavity QED is a two-level emitter interacting with a high-quality factor single-mode optical resonator. The hybridization of the emitter and photon wave functions mandates large vacuum Rabi frequencies and long coherence times; features that so far have been successfully realized with trapped cold atoms and ions, and localized solid-state quantum emitters such as superconducting circuits, quantum dots, and color centers Reiserer and Rempe (Rev Modern Phys 87:1379, 2015), Faraon et al. (Phys Rev 81:033838, 2010). Thermal atoms, on the other hand, provide us with a dense emitter ensemble and in comparison to the cold systems are more compatible with integration, hence enabling large-scale quantum systems. However, their thermal motion and large transit-time broadening is a major bottleneck that has to be circumvented. A promising remedy could benefit from the highly controllable and tunable electromagnetic fields of a nano-photonic cavity with strong local electric-field enhancements. Utilizing this feature, here we investigate the interaction between fast moving thermal atoms and a nano-beam photonic crystal cavity (PCC) with large quality factor and small mode volume. Through fully quantum mechanical calculations, including Casimir–Polder potential (i.e. the effect of the surface on radiation properties of an atom), we show, when designed properly, the achievable coupling between the flying atom and the cavity photon would be strong enough to lead to quantum interference effects in spite of short interaction times. In addition, the time-resolved detection of different trajectories can be used to identify single and multiple atom counts. This probabilistic approach will find applications in cavity QED studies in dense atomic media and paves the way towards realizing large-scale, room-temperature macroscopic quantum systems aimed at out of the lab quantum devices.

## 1 Introduction

The field of cavity quantum electrodynamics (CQED) dates back to more than 50 years ago when Purcell in his seminal work reported that the radiation properties of an atom can be modified via its surroundings [3]. Within the last decades CQED has been a versatile and powerful testbed to investigate fundamental postulates of quantum mechanics such as superposition and entanglement [4, 5]. In addition,

it has been the source of various developments in the fields of quantum technologies and quantum information [1, 6–8].

Early CQED experiments were considering the modification of the atom lifetime and its radiation properties in the vicinity of a low-quality factor cavity. However, with the development of high finesse cavities, most of CQED studies shifted towards exploring *strong coupling* regime where the energy between the atom and cavity photon is exchanged coherently. Within that regime and starting with microwave CQED, entanglement between highly excited Rydberg atoms flying across superconducting cavities and microwave photons was observed [9]. Later, by combining low-lying atomic transitions and high-finesse dielectric cavities strong atom–photon couplings in the visible range was demonstrated [10–16].

The introduction of nano-photonics to the field of quantum optics and atomic physics has substantially broadened the capabilities of atom–photon systems. Nano-photonic and plasmonic structures provide quantum emitters with a large tailorability of the local density of the optical states (LDOS),

---

This article is part of topical collection on Optical Nanofibers and Microresonators.

---

✉ Hadiseh Alaeian  
alaeian@pi5.physik.uni-stuttgart.de

<sup>1</sup> 5 Physikalisches Institut, University of Stuttgart, Pfaffenwaldring 57, 70569 Stuttgart, Germany

<sup>2</sup> Center for Integrated Quantum Science and Technology (IQST), Stuttgart, Ulm, Germany

hence making a unique platform for studying well-designed and controllable atom–light interaction. In addition, quantum optical platforms can exploit the typical high-quality factor (Q) and the small mode volume of photonic modes of nano-photonic devices to explore the very large cooperative coupling regimes. Such unique capabilities have been actively investigated in various solid-state systems such as quantum dots [2, 17, 18], color centers [19, 20], and embedded rare-earth ions [21, 22]. Each of these platforms has its strength and weaknesses and might be suitable only for specific problems.

However, unless particular treatments are considered, in most of these systems, the coupling of quantum emitters to phonons of the host material causes large inhomogeneous broadening for the emitters which is a major bottleneck in these atom-like cavity systems.

On the other hand, atoms are naturally identical quantum emitters so the system composed of these quantum emitters combined with nano-photonic devices would substantially improve the inhomogeneous broadening of these hybrid systems [23, 24]. Therefore, the hybrid quantum systems of atoms and nano-photonic devices have a promising perspective for exploring new realms of CQED. Within the last 2 decades and with the advancements of nano-photonics and nano-technology, quantum optics has witnessed a lot of efforts focused on interfacing these structures with neutral atoms [25–31].

Among the various nano-photonic devices photonic crystal (PhC) cavities are some of the most promising candidates to obtain high-Q resonances and small mode volume, simultaneously. They are generally designed by creating an optical defect in the bandgap of a structure with periodic modulation of the refractive index. Popular designs are based on a 2D PhC, where one or several holes are removed from the otherwise periodic lattice [32–35]. The propagating mode of the waveguide at the center becomes evanescent at the edges and is thus confined, forming a resonant mode. Cavities are also obtained in 1D PhC and usually are made in a ridge waveguide in which a series of air holes are etched. The two series are usually separated by a distance  $L$  forming a cavity, where light is trapped.

In this article, we present the theoretical proposal of a CQED system based on thermal atoms coupled to 1D nano-beam cavity where a periodic spatial modulation in dielectric distribution is arranged over a dielectric nano-beam. The properties of such a photonic crystal have been exploited to engineer the optical dispersion. As suggested by our numerical calculations even in the presence of the inhomogeneous broadening of the thermal atoms and the large transit time broadening, a strong coupling between the atom and the cavity photon is expected. We also calculate some of the important atom-surface effects, like the Casimir–Polder potential, to incorporate the surface effects on the atoms. Moreover,

we extend the study further to include the behavior of more than one atom in the vicinity of the cavity and show that the temporal and spectral information can be used to distinguish between different cases.

## 2 Photonic crystal cavity

The structure of our interest is a suspended silicon nitride (SiN) nano-beam with width  $w$  and thickness  $h$ . A 1D array of air holes with radius  $r$  and periodicity  $a$  modulates the refractive index of this waveguide as schematically shown in Fig. 1. Rubidium (Rb) atoms with thermal velocity  $\vec{v}$  and Maxwell–Boltzmann distribution fly in the vicinity of the nano-device along random trajectories as denoted by black arrows in Fig. 1. The structure is assumed to be excited with coherent light via input grating couplers (In). The transmitted light, after interacting with the atoms, will be collected from another grating coupler at the output (Out) and sent to a fast single photo diode.

The periodic modulation of the refractive index of the nano-beam in 1D leads to a partial photonic bandgap along the  $x$ -direction. Within the frequencies of our interest, i.e. near-infrared, SiN can be treated as a dispersion-less material with fixed refractive index [36],  $n_{\text{SiN}} = 2.05$ . Figure 2a shows the band structure of such 1D periodic structure, with  $w = 420$  nm,  $h = 250$  nm,  $a = 325$  nm, and  $r = 91$  nm, in the first Brillouin zone  $[0, \pi/a]$ . With these parameters the structure supports a wide photonic bandgap with band edges at  $\lambda = 881$  nm and  $\lambda = 754$  nm for the dielectric (DB) and air band (AB), respectively. This wide bandgap implies that the periodic array of the holes serves as a good mirror for the photons within that energy range. These regions, indicated as mirror in Fig. 1, trap the photons for a long time in the cavity section ( $\tau_{ph}$  is on the order of ns). By optimizing the positions and radii of the holes in the middle part a defect center can be realized that supports a single, high-quality factor resonance. Since the atoms fly through the holes, the field intensity should be confined mostly inside the air holes; hence, the resonance frequency should be close to the air band (AB). In addition, to achieve the longest photon lifetime within the cavity, the spatial profile of the resonant mode should have a Gaussian distribution to minimize the leakage of the photons out of the cavity. These conditions result in the radii of  $r = 63, 67, 73,$  and  $81$  nm for the holes in the cavity region. These parameters lead to a resonant mode at  $780$  nm, i.e.  $D_2$ -line transition of Rb. Figure 2b, c shows the field intensity profile of the cavity mode at three different cross sections. As can be seen the resonant mode is tightly confined within the cavity region close to the nano-beam and is mainly polarized along the  $y$ -direction.

From these mode profiles, we can calculate the relevant CQED parameters of this atom-cavity system. Our numerical

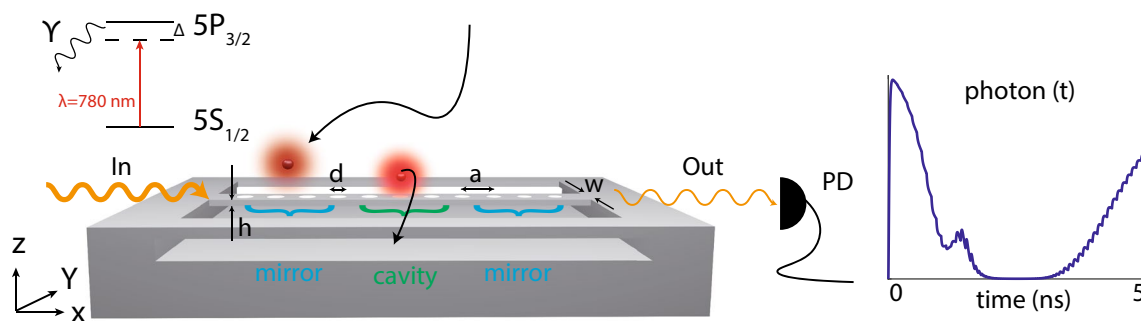
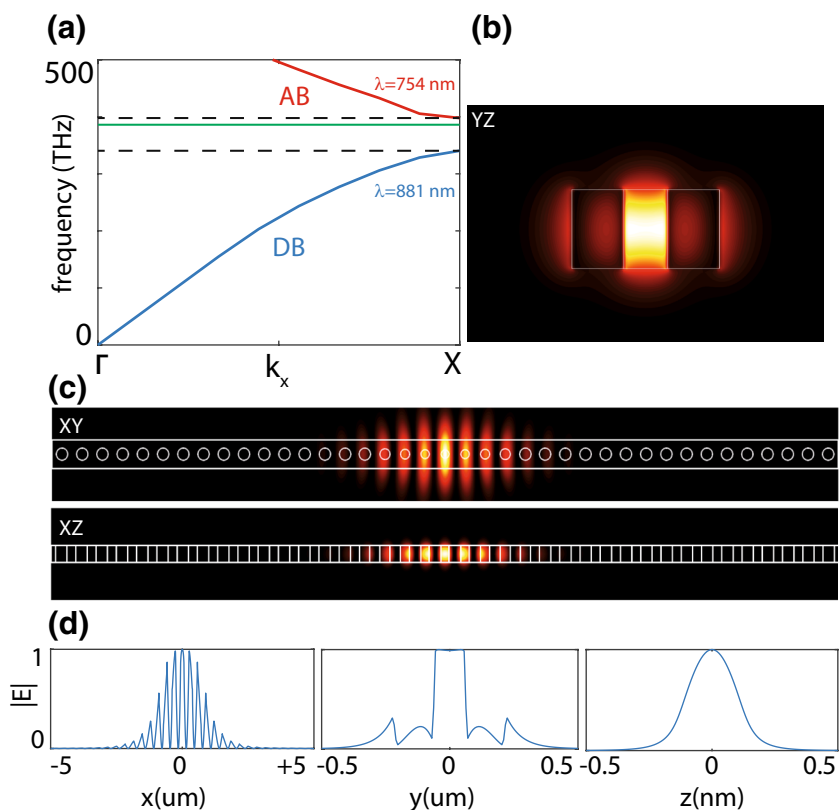


**Fig. 1 a** Schematics of the nano-beam photonic crystal cavity composed of a slab with width  $w$  and height  $h$  modulated with 1D array of holes with radius  $r = d/2$  and periodicity  $a$  in the mirror section. The electronic energy levels of rubidium atoms flying along random trajectories in the vicinity of the structure has been shown as well. A

pair of grating couplers at input and output will be used to excite the device with a coherent light (In) and collect the scattered light (Out) from the device and send it to a single-photon detector. The graph shows an example of the time-trace of the photons measured by photo diode

**Fig. 2 a** Photonic band-diagram of a 1D periodic hole array in a SiN nano-beam within the first Brillouin zone. The dashed lines show the photonic bandgap edges and DB and AB solid lines show the dielectric band and air band, respectively. The green line (horizontal solid line) shows the cavity resonance frequency with respect to the band edges. Electric field intensity profile of the cavity mode in **b** YX and **c** XY, XZ cross sections. The solid white lines in panels **b**, **c** show the physical boundaries of the structure. **d** 1D electric field amplitude profiles along  $x$ ,  $y$ ,  $z$ -directions at the central planes



calculations indicate the quality factor of  $Q = 65,000$  equivalent to a photon decay rate of  $\kappa_{ph} \approx 3.7 \times 10^{10}$  1/s.

Aside from the Q-factor, mode volume is another important indication of the atom–photon coupling strength. For a dispersion-less material like SiN the mode volume is determined by

$$V_{\text{mode}} = \frac{\int_V dV \epsilon(\vec{r}) |\vec{E}(\vec{r})|^2}{\text{Max}(\epsilon(\vec{r}) |\vec{E}(\vec{r})|^2)}, \tag{1}$$

where  $\epsilon(\vec{r})$  is distribution of the structure permittivity as a function of position and  $\vec{E}(\vec{r})$  is the electric field profile [37].

Due to the sub-wavelength features of the mode profile the vacuum Rabi frequency is highly position dependent and its maximum in the middle of the central hole is given by

$$g_{\max} = \sqrt{\frac{\omega_{res}}{2\hbar\epsilon_0 V_{\text{mode}}}} \cdot d_{sp}, \tag{2}$$

where in the above relation  $\epsilon_0$  is the vacuum permittivity and  $d_{sp}$  is the effective transition dipole moment of Rb at 780 nm in a linearly polarized field.

To determine the effective transition dipole moment and due to the degeneracy of Zeeman sub-levels one had to average over all allowed transition [38]. As the cavity field is linearly polarized the average should be performed on  $\pi$ -allowed transitions, only.

$$d_{sp}^2 = \frac{\sum_{m_{F'}} |C_{m_{F'}}|^2}{2F + 1} \langle J || e r || J' \rangle^2, \tag{3}$$

where in general in the above equation  $C_{m_{F'}}$  is the Clebsch–Gordan coefficients of transitions from  $m_F$  magnetic sub-level of the ground state to  $m_{F'}$  magnetic sub-level in the excited state. (For  $\pi$ -polarization field  $m_F = m_{F'}$ .) In addition,  $D = \langle J || e r || J' \rangle$  is the reduced dipole moment of  $D_2$ -transition and is related to the excited-state lifetime as [39].

$$\langle J || e r || J' \rangle^2 = \frac{3\pi\epsilon_0 \hbar c^3}{\omega_{sp}^2} \frac{2J' + 1}{2J + 1} \Gamma_{sp}, \tag{4}$$

where  $D = 3.584 \times 10^{-29}$  C.m for rubidium atoms. Using Eq. 3, the effective transition dipole moment will be determined as  $d_{sp} = 1.6584 \times 10^{-29}$  C.m.

The atom is flying through the device and will experience a transit-time broadening due to its finite interaction time with the field. For an atom at room temperature with the r.m.s velocity of  $\sigma = \sqrt{3k_B T / m_{Rb}} \approx 295$  m/s, the broadening due to the finite interaction time with the cavity field can be approximated as

$$\tau_{\text{int}} = \frac{h}{\sigma} \approx 0.9 \text{ ns}, \tag{5}$$

where in the above equation  $h$  is the slab height which is the shortest interaction length of the atom and the cavity. This is just an order of magnitude calculation to estimate the achievable atom–photon cooperativity expected from this cavity. The effect of this transient interaction between the atom and the cavity field is properly modeled via Monte Carlo calculations presented in Sect. 4.

From these values, we can estimate the cooperativity of this atom-cavity system at the cavity center, a parameter that indicates the ratio between all the coherent and incoherent effects in a coupled system, and is determined as

$$C = 2 \frac{g_{\max}^2}{\kappa_{\text{ph}} \Gamma_{\text{atom}}} \approx 406. \tag{6}$$

Table 1 summarizes the important parameters of this cavity-atom system.

**Table 1** CQED parameters of the nano-beam photonic crystal cavity

$\lambda_{res}$	$V_{\text{mode}}$	$Q$	$g_{\max}$	$\kappa_{\text{ph}}$	$C$
780 nm	$0.08 \lambda_{res}^3$	65,000	$2\pi \times 15$ GHz	$2\pi \times 5.9$ GHz	406

### 3 Body-assisted Green’s function

#### 3.1 Local density of the optical states (LDOS)

As stated in the previous section, the cavity has a large quality factor ( $Q$ ) and a small mode volume hence the radiation properties of an atom in the vicinity of the structure would be strongly modified. One of the interesting aspects of nano-photonic devices is their ability to substantially modify the local density of the optical states (LDOS) due to the large gradient of the field profile on the order of or below the resonance wavelength.

The modification of an emitter properties in the vicinity of the structure occurs in two ways: 1. via changing the decay rate of the emitter by a factor known as the Purcell factor. 2. Via modifying the electronic levels of the emitter. Since the refractive index of the device is rather large there would be a noticeable dipole–dipole interaction potential between the emitter and its image. This Casimir–Polder interaction induces a shift in the atomic line [40]. As both of these phenomena are related to the body-assisted Green’s function, in this section, we present the Green’s function and calculate its corresponding Casimir–Polder potential.

The electromagnetic Green’s tensor denoted as  $\mathbf{G}(r, r'; \omega)$  is the electric field at location  $r$  generated by an infinitesimal current moment at location  $r'$  and at frequency  $\omega$ . In other words, it is the impulse response of the Helmholtz operator determined via the following equation:

$$\left( \nabla^2 - \left( \frac{\omega}{c} \right)^2 \epsilon(r) \right) \mathbf{G}(r, r'; \omega) = \vec{\delta}(r - r'), \tag{7}$$

where in the above equation  $\epsilon(r)$  is the spatial distribution of the permittivity set by the nano-photonic device geometry.

Closed formulae for Green tensors are merely available for highly symmetric geometries; hence, in general, for most of the systems it should be determined numerically. In this work, we employed *Lumerical* an FDTD-based commercial software to solve this equation numerically.

The Green’s tensor is also an indication of the radiated power from the dipole in the system. Therefore, the larger the coupling to the modes the larger radiated power by the dipole. As mentioned in the previous section, for this nano-beam geometry, the cavity mode is mainly polarized along the  $y$ -direction, specifically in the  $XY$  plane of symmetry. This implies that the best coupling to various dipole orientations can be obtained for a  $y$ -directed dipole, the dipole

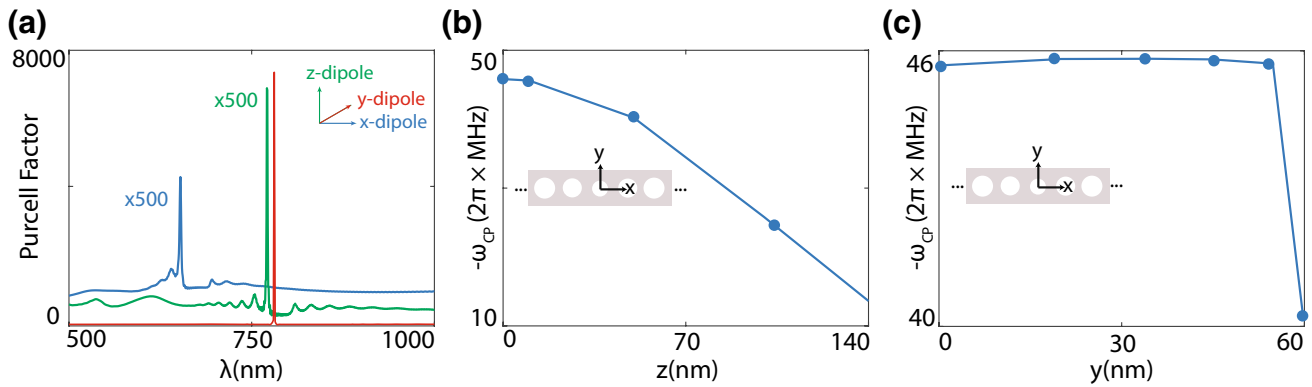


**Fig. 3** **a** Purcell factor enhancement of a radiating electric dipole at the center of the cavity, i.e.  $x = y = z = 0$  as a function of the dipole wavelength. The blue, red, and green lines correspond to the  $x$ ,  $y$ , and  $z$ -oriented electric dipoles. Purcell factors of  $x$ - and  $z$ -oriented dipoles are multiplied by a factor 500 to have comparable values to the  $y$ -dipole case. **b** Casimir–Polder-induced line shift as a function

of  $z$ , away from the device surface, for an electric dipole at  $x = y = 0$ . The slab height  $h = 250$  nm. The induced potential is calculated for a dipole emitting at  $D_2$  line of rubidium. **c** Casimir–Polder-induced line shift as a function of  $y$ , along the beam width, for an electric dipole at  $x = z = 0$ . The radius of the central hole  $r = 63$  nm. The filled circles in each case show the simulated data points

oriented along the beam width. For the other two orientations, the radiated power is substantially lower, as the dipole and the cavity mode do not couple efficiently. This qualitative prediction can be clearly observed in the numerical calculations presented in Fig. 3a where the calculated Purcell factor for all of the  $x$ -,  $y$ - and  $z$ -oriented dipoles has been shown as a function of the dipole wavelength. As can be observed, the power emitted from a  $y$ -directed dipole substantially increases when the dipole energy approaches the cavity resonance wavelength. Moreover, the emitted power is noticeably higher compared to the power emitted from  $x$ ,  $z$ -directed dipoles. Note that the radiated powers from the latter dipoles are not strictly zero since aside from the cavity mode, there are continuum of leaky modes that the dipoles could always couple to. The finite spikes in the radiation spectrum of the  $x$ -,  $z$ -oriented electric dipoles are due to some parasitic cavity effects in a finite-sized structure we considered in all of the simulations.

### 3.2 Casimir–Polder effect

When an emitter radiates in the vicinity of a large-index dielectric surface its radiation properties not only will be affected by the change of the local density of the optical states (LDOS) as discussed in the previous part, but also its electronic levels will be affected by a dipole–dipole interaction between the atom and its induced dipole image. This phenomenon known as Casimir–Polder potential is closely related to the modification of the emission properties of the dipole locally and is related to the Green’s function via the following relation [41]:

$$U_{CP}^{(n)}(r) = -\frac{\hbar}{2\pi} \mu_0 \mathcal{P} \int_0^\infty \text{Im}(\text{Tr}(\alpha_n(\omega) \mathbf{G}_{sc}(r, r; \omega)) \omega^2) d\omega, \quad (8)$$

where  $\mathbf{G}_{sc}(r, r; \omega)$  is the scattered part of the Green’s tensor ( $\mathbf{G}_{sc} = \mathbf{G} - \mathbf{G}_{\text{free space}}$ ) as defined in the previous section and  $\alpha_n(\omega)$  is the dynamical polarizability tensor of the emitter at frequency  $\omega$  and in the  $|n\rangle$ -state. Symbol  $\mathcal{P}$  in front of the integral emphasizes that one has to calculate the Cauchy principal value of the integral. This is important as we need to calculate the Casimir–Polder potential of an excited atom in the vicinity of the structure, where  $\alpha_p(\omega)$  has a pole at  $D_2$ , corresponding to a real photon emission. Due to the large velocity of the atoms in a thermal gas the force exerted by  $U_{CP}$  and its effect on altering the atomic trajectory can be ignored. Therefore, one only needs to include the effect of this potential on shifting the atomic resonance as  $\hbar\omega_{CP} = U_{CP}$ .

In general, the induced potential consists of resonant and non-resonant parts. While the former is related to all of the virtual transitions from the emitter the latter is related to the real transitions of an atom in the  $|n\rangle$ -state. Unless the emitter is very close to the body, often the contribution from real photons exceeds the virtual photon parts [41]. In addition, as suggested by the results in Fig. 3a, the body-assisted Green’s function of this system is mainly peaked at the emitter resonance wavelength (i.e.  $\lambda_{\text{res}}$ ), suggesting a further increase due to the LDOS. Therefore, for such a high-Q, single mode cavity we can limit ourselves to the resonant part and approximate the Casimir–Polder potential with the body-assisted Green’s function in the vicinity of its resonance.

Employing this approximation and calculating the polarizability from the transition dipole moments and frequencies,

we have calculated the Casimir–Polder potential at several positions close to the device. In Fig. 3b, c, we show some of the calculated results of the frequency shift due to the Casimir–Polder effect ( $\omega_{CP}$ ) away from the structure along the  $z$ -direction, and away from the cavity towards the hole edge along the  $y$ -direction, respectively. As can be seen, due to the induced dipole image, a Rb atom radiating at  $D_2$  experiences about tens of MHz line shifts in the transition frequency. Also due to the attractive force between the dipole and its image the shift in the energy is always negative. Comparing these values with the transit broadening an atom experiences as it flies through the structure it can be concluded that the Casimir–Polder potential does not have a large effect. Indeed, the effect becomes more and more pronounced for slower atoms where the energy shift can lead to measurable detuning between the atom and cavity hence, diminishing the strong coupling between them.

#### 4 Atom–light interactions and Monte-Carlo simulations

In the previous sections, we conducted some orders of magnitude estimation of the atom photon coupling as well as more quantitative investigations on the Casimir–Polder potential to explore the behavior of a moving atom in the vicinity of well-designed high-Q PCC with small mode volume. Those analyses suggest that the achievable coupling between a flying atom and a photon cavity is strong enough to expect quantum interference effects from this hybrid system even though moving atoms are typically subject to the large transit-time broadening. To fully evaluate the performance of the hybrid system, however, one needs to treat the atom–photon coupling more accurately. In this section, we employ a Monte Carlo scheme that combines the spatially varying photon field and the Casimir–Polder potential derived in the previous section with full quantum mechanical description of the atom–photon coupling to investigate the interaction of a moving atom with the nano-cavity. We investigate the motion of a thermal atom with a random velocity  $\vec{v}$  following a random trajectory  $\vec{r}(t)$  determined by its velocity. The evolution of the joint density matrix of the atom and photon at each time is determined via the following Liouville’s equation:

$$\begin{aligned} \frac{d\rho}{dt} = & -i[H, \rho] + \kappa \left( a\rho a^\dagger - \frac{1}{2} \{ a^\dagger a, \rho \} \right) \\ & + \Gamma \left( \sigma^- \rho \sigma^+ - \frac{1}{2} \{ \sigma^+ \sigma^-, \rho \} \right), \end{aligned} \tag{9}$$

where  $(\kappa, \Gamma)$  are the photon decay rate from the cavity and the atom lifetime in the excited state, respectively.  $a, a^\dagger$  are the annihilation and creation operators of the photon field,

and  $\sigma^-, \sigma^+$  are the atomic lowering and raising operators, respectively.

Atom–photon interaction can be properly studied with Fock states and we investigate the scenario where photons are injected with a weak, coherent excitation at the rate  $\epsilon_L$ . Therefore, the total Hamiltonian in the rotated frame of the laser is given via the following driven Jaynes–Cumming form as

$$\begin{aligned} H = & (\omega_c - \omega_L) a^\dagger a + (\omega_a(t) - \omega_L) \sigma^+ \sigma^- \\ & + (g(t) a \sigma^+ + g^*(t) \sigma^- a^\dagger) + \epsilon_L (a + a^\dagger), \end{aligned} \tag{10}$$

where  $\omega_c, \omega_a, \omega_L$  are the cavity, atom, and laser frequency, respectively, and  $g(t)$  is the vacuum Rabi coupling of the atom-cavity at atom position of  $r(t)$  and varies as the atom moves along the device. Also, due to the Casimir–Polder effect, the detuning between the atom and the laser is position and, therefore, time dependent as well. We would like to emphasize that using a complex Rabi coupling, as  $g(t)$ , the effect of position dependence of the photonic mode phase has been inherently included.<sup>1</sup>

Figure 4 shows the results of the Monte Carlo simulation for a moving atom in the vicinity of PCC for three different velocities and initial position. The joint density matrix has been evolved according to the above equation and the instantaneous expectation value of the intra-cavity photon numbers  $\langle a^\dagger a \rangle$  has been calculated for different cavity-laser detuning values ( $\Delta_{cL}$ ) while the atom moves in the vicinity of the cavity. The interaction time and the coupling strength between atom and cavity strongly depend on the atom velocity and its initial position; hence, the behavior drastically changes along different trajectories. The time-averaged photon number as a function of cavity-laser detuning has been shown in the second row for each case. The third row manifests the change of the intra-cavity photon number as a function of time when  $\Delta_{cL}=0$ . As can be observed the number of photons in the cavity drops when the coupling between the atom and the cavity photon is strong enough to induce a large detuning between the input laser frequency and the frequencies of the dressed states. In other words, the cavity becomes opaque to the input laser for a finite amount of time. The inverse scenario is observable as well. At large cavity-laser detuning, the presence of atom makes the cavity transparent for a while.

To produce a gated cloud of atoms one can employ the light-induced atomic-desorption (LIAD) process. In the

<sup>1</sup> For a traveling wave with well-defined wave vector ( $\vec{k}$ ), hence a linear phase change in space, this is the well-known Doppler shift as  $\omega_D = \vec{k} \cdot \vec{v}$ . However, due to the sub-wavelength features of the cavity field the phase is better to be included numerically and on the same ground as its amplitude.

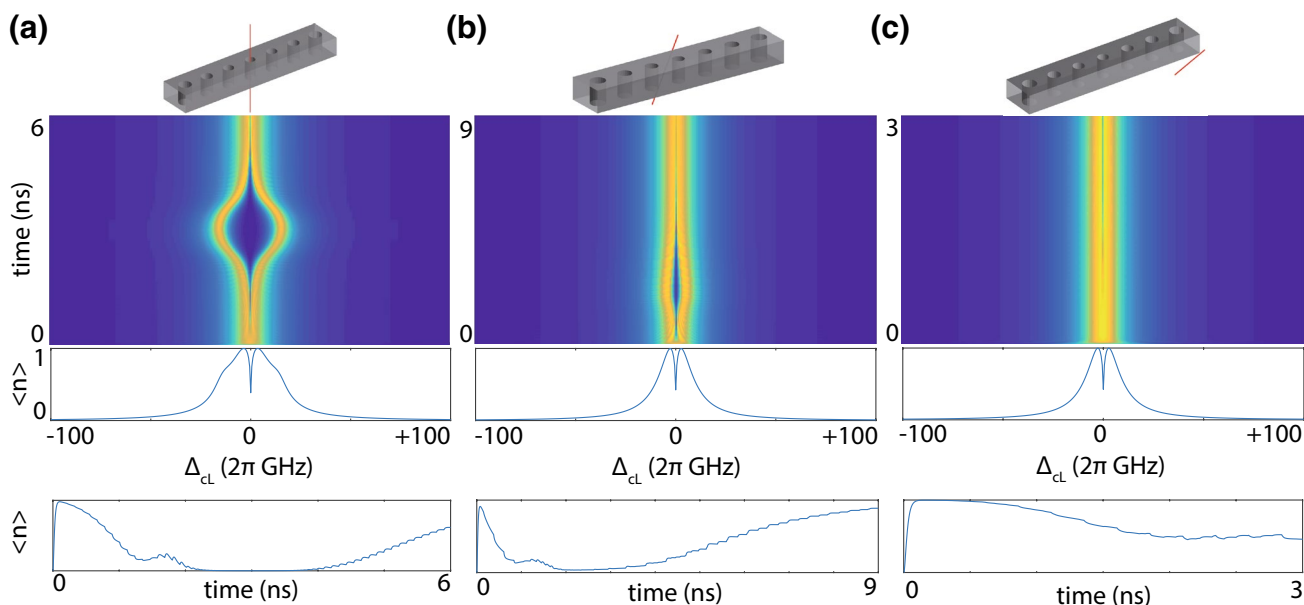


**Fig. 4** Instantaneous photon numbers  $\langle a^\dagger a \rangle$  of moving atoms as a function of cavity-laser detuning ( $\Delta_{cl}$ ) for an atom **a**  $r_0 = (0 \ 0 \ 600)$  nm and  $v_0 = (0 \ 0 \ -200)$  m/s, **b**  $r_0 = (100 \ 150 \ 300)$  nm and  $v_0 = (0 \ 50 \ -100)$  m/s, and **c**  $r_0 = (800 \ -200 \ -500)$  nm and  $v_0 = (120 \ -40 \ 100)$  m/s. In each case, the simulation has been terminated when an atom crashes onto the device or the simulation boundaries. The schemat-

ics on top in each case show the atom trajectory alongside the photonic crystal cavity. In each sub-figure, the color-map panel shows the real-time variation of the intra-cavity photon number, the middle row shows the averaged signal over time as a function of the cavity-laser detuning, and lower panel shows the time signal at zero detuning ( $\Delta_{cl} = 0$ )

LIAD process, also known as the photo-electric effect for atoms, high-energy laser pulses hit the wall of an atomic vapor cell, which is coated with alkali atoms and desorb them from the surface [42–45]. When chosen properly atomic clouds as dense as  $1000 \text{ atoms}/\mu^3$  can be generated [46]. The inset of Fig. 5 shows the typical trajectory of atoms released from the wall via LIAD process. Figure 5 shows the normalized intra-cavity photon number as a function of cavity-laser detuning after averaging over 100,000 atom trajectories. Due to the random paths, which give different atom–photon coupling, the dressed state splitting is trajectory dependent. However, the averaged vacuum Rabi coupling is still large enough to lead to the spitting of majority of fast moving atoms at  $\Delta_{cl} = 0$  as they transiently pass through the cavity. We would like to emphasize that the observed dip at zero detuning here is different from DIP (dipole-induced transparency) studied in the overdamped atom-cavity and plasmonic systems [47–49]. While DIP is a steady-state feature of those coupled systems the transparency window observed in the atomic ensemble here appears for thermal atoms transiently interacting with the field and far from their steady state.

The analysis can be extended further to investigate the behavior of multiple atoms interacting with the same cavity mode. Figure 6a–c shows the instantaneous number of intra-cavity photons as a function of cavity-laser detuning for three different delays between two atoms for  $\delta t = 0, 2, 4$  ns,

respectively. The complete study of the many-atom cavity coupling in the dense atomic media is the topic of follow-up studies and as very different scenarios are imaginable here we only limit ourselves to atoms flying through the central hole, where the interaction is the strongest. In all of these

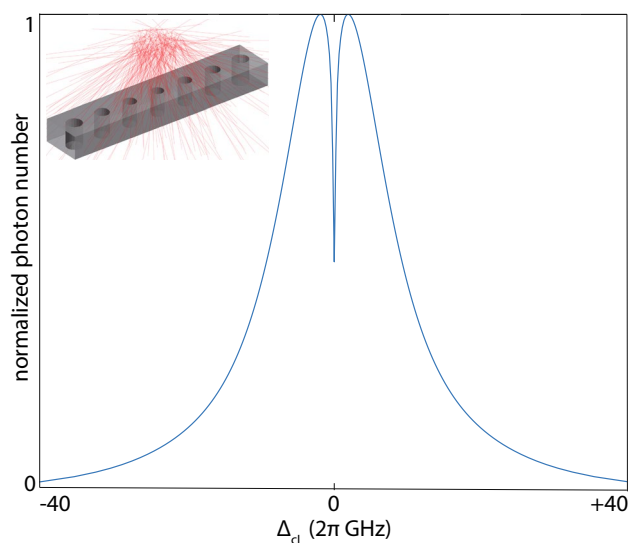


**Fig. 5** Normalized photon number as a function of laser-cavity detuning  $\Delta_{cl}$ , averaged over 100,000 trajectories generated from light-induced atomic desorption (LIAD) process. The inset shows some of the trajectories of released atoms

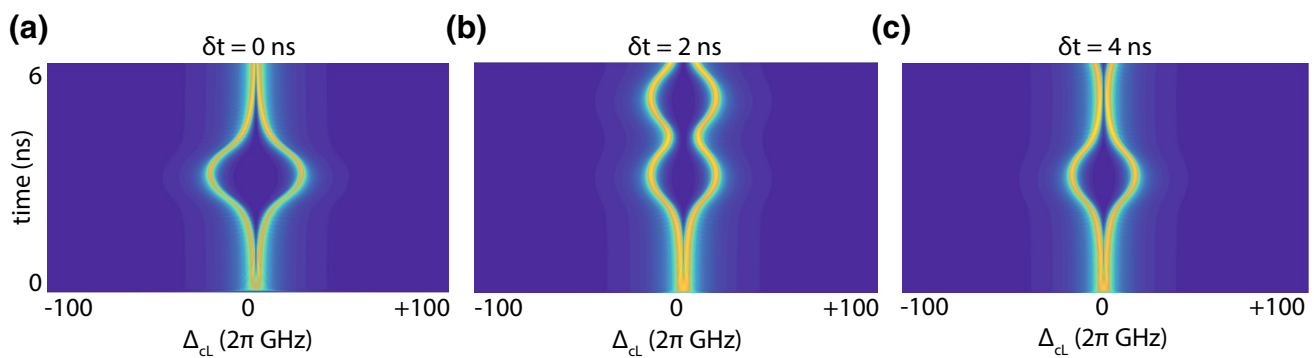


**Fig. 6** Instantaneous intra-cavity photon number as function of cavity-laser detuning ( $\Delta_{cl}$ ) when two atoms fly through the central hole. Both atoms have the same velocity of  $\vec{v} = -200\hat{z}$  m/s and

move towards the cavity along the same trajectory. However, they are delayed by  $\delta t$  **a** 0 ns, **b** 2 ns and **c** 4 ns

cases, the atoms follow the same trajectory along the line passing through the center of the cavity with the velocity of  $\vec{v} = -200\hat{z}$  m/s. As can be seen depending on the delay between atoms the behavior is substantially different. When there is no delay and both atoms fly in the vicinity of the cavity simultaneously the behavior is similar to the single atom case (Fig. 4a) except an increase in the effective Rabi coupling by  $\sqrt{2}$ . When there is a finite delay between atoms, as depicted in Fig. 6b, c, the first atom can make the cavity opaque while the second atom can allow the photons to enter the cavity again. This behavior, which is strongly delay dependent, is depicted in panels (b) and (c) where multiple oscillations in the instantaneous photon number can be observed. For longer delays the first atom is already far away from the cavity and its effect is so negligible that the second atom can be treated almost, independently.

## 5 Conclusion

In this work, we proposed a new hybrid system for CQED studies with thermal atoms. Compared to their cold atom counterparts, thermal atoms are less controllable and fly along random paths. However, some pre-selection schemes such as geometrical treatments on the fabricated device, on-chip collimators [50], or dense LIAD generated clouds can be employed to limit the atomic trajectories to more favorable ones.

To overcome the typical problem of short interaction time between flying atoms and the cavity mode, we designed a high-quality factor photonic crystal cavity that provides large vacuum Rabi coupling and cooperativity. We studied the effect of cavity and LDOS modification in controlling the decay rate. In addition, we calculated the surface effect and Casimir–Polder effect in altering the atomic transitions. Using a Monte Carlo algorithm and combining the full quantum-mechanical description of atom–photon interaction

with Casimir–Polder effects, we investigated the feasibility of observing coherent coupling between a flying atom and the cavity photon. Our results predict that the attainable coupling can be large enough to achieve the strong coupling regime in spite of all decoherence and transit time effects. In addition, we extended the study to more than one atom case and investigated multiple atom-induced transparency occasions that can be achieved in this system.

Our designs and analysis set the foundations for investigating atom–photon interactions in more complicated nanophotonic devices that support specific features such as topology or chirality [51]. Furthermore, due the large attainable LDOS in nano-devices the coupling of atoms to non-desired modes will be substantially suppressed and photon-mediated coupling between atoms are expected to be enhanced. Interfacing atoms with custom nano-photonic devices is a burgeoning emerging field and new eras of quantum optics are ahead, which leads to novel types of interactions between the atoms and the engineered photonic states.

**Acknowledgements** Open Access funding provided by Projekt DEAL. The authors thank Stefan Scheel and Helge Dobbertin for several fruitful discussions, and Mark Zentile for his diligent reading of this work. H.A. acknowledges the financial support from IQST Young Investigator Grant and the Elite programme from Baden-Württemberg Stiftung.

**Open Access** This article is licensed under a Creative Commons Attribution 4.0 International License, which permits use, sharing, adaptation, distribution and reproduction in any medium or format, as long as you give appropriate credit to the original author(s) and the source, provide a link to the Creative Commons licence, and indicate if changes were made. The images or other third party material in this article are included in the article's Creative Commons licence, unless indicated otherwise in a credit line to the material. If material is not included in the article's Creative Commons licence and your intended use is not permitted by statutory regulation or exceeds the permitted use, you will need to obtain permission directly from the copyright holder. To view a copy of this licence, visit <http://creativecommons.org/licenses/by/4.0/>.



## References

1. A. Reiserer, G. Rempe, Cavity-based quantum networks with single atoms and optical photons. *Rev. Mod. Phys.* **87**, 1379 (2015)
2. A. Faraon, A. Majumdar, J. Vuckovic, Generation of nonclassical states of light via photon blockade in optical nanocavities. *Phys. Rev. A* **81**, 033838 (2010)
3. E.M. Purcell, H.C. Torrey, R.V. Pound, Resonance absorption by nuclear magnetic moments in a solid. *Phys. Rev.* **69**, 37 (1946)
4. W.P. Schleich, Quantum optics: optical coherence and quantum optics. *Science* **727**, 1897 (1996)
5. J.M. Raimond, M. Brune, S. Haroche, Colloquium: Manipulating quantum entanglement with atoms and photons in a cavity. *Rev. Mod. Phys.* **73**, 565 (2001)
6. H. Walther, B.T.H. Varcoe, B.-G. Englert, T. Becker, Cavity quantum electrodynamics. *Reposrts Prog. Phys.* **69**, 1325 (2006)
7. S. Haroche, "A short history of cavity quantum electrodynamics," in *Conference on Coherence and Quantum Optics 2007*, (Rochester, NY, USA), Optical Society of America, (2007)
8. H. J. Kimble, "The quantum internet," *Nature*, pp. 1023–1030, (2008)
9. L. Davidovich, N. Zagury, M. Brune, J.M. Raimond, S. Haroche, Colloquium: manipulating quantum entanglement with atoms and photons in a cavity. *Phys. Rev. A* **50**, 895 (1994)
10. G. Rempe, R.J. Thompson, R.J. Brecha, W.D. Lee, H.J. Kimble, Optical bistability and photon statistics in cavity quantum electrodynamics. *Phys. Rev. Lett.* **67**, 1727 (1991)
11. R.J. Thompson, G. Rempe, H.J. Kimble, Observation of normal-mode splitting for an atom in an optical cavity. *Phys. Rev. Lett.* **68**, 1132 (1992)
12. P. Munstermann, T. Fischer, P. Maunz, P.W.H. Pinkse, G. Rempe, Dynamics of single-atom motion observed in a high-finesse cavity. *Phys. Rev. Lett.* **82**, 3791 (1999)
13. C.L. Hung, S.M. Meenehan, D.E. Chang, O. Painter, H.J. Kimble, Trapped atoms in one-dimensional photonic crystals. *New J. Phys.* **15**, 083026 (2013)
14. C.J. Hood, T.W. Lynn, A.C. Doherty, A.S. Parkins, H.J. Kimble, The atom-cavity microscope: single atoms bound in orbit by single photons. *Science* **287**, 1447–1453 (2000)
15. J.D. Thompson, T.G. Tiecke, N.P. de Leon, J. Feist, A.V. Akimov, M. Gullans, A.S. Zibrov, V. Vuletic, M.D. Lukin, Coupling a single trapped atom to a nanoscale optical cavity. *Science* **340**, 1202–1205 (2013)
16. J. Lee, G. Vrijsen, I. Teper, O. Hosten, M.A. Kasevich, Many-atom-cavity qed system with homogeneous atom-cavity coupling. *Opt. Lett.* **39**, 4005 (2014)
17. D. Englund, A. Faraon, I. Fushman, N. Stoltz, P. Petroff, J. Vuckovic, Controlling cavity reflectivity with a single quantum dot. *Nature* **450**, 857 (2007)
18. A. Faraon, A. Majumdar, D. Englund, E. Kim, M. Bajcsy, J. Vuckovic, Integrated quantum optical networks based on quantum dots and photonic crystals. *New J. Phys.* **13**, 055025 (2011)
19. M. Radulaski, M. Widmann, M. Niethammer, J. L. Zhang, S.-Y. Lee, T. Rendler, K. G. Lagoudakis, N. T. Son, E. Janzen, J. W. Takeshi Ohshima, J. Vuckovic, Scalable quantum photonics with single color centers in silicon carbide. *Nano Lett.* **13**, 1782 (2017)
20. J.L. Zhang, S. Sun, M.J. Burek, C. Dory, Y.-K. Tzeng, K.A. Fischer, Y. Kelaita, K.G. Lagoudakis, M. Radulaski, Z.-X. Shen, N.A. Melosh, S. Chu, M. Loncar, J. Vuckovic, Strongly cavity-enhanced spontaneous emission from silicon-vacancy centers in diamond. *Nano Lett.* **18**, 1360 (2018)
21. Y.-H. Chen, X. Fernandez-Gonzalvo, J.J. Longdell, Coupling erbium spins to a three-dimensional superconducting cavity at zero magnetic field. *Phys. Rev. B* **94**, 075117 (2016)
22. E. Miyazono, I. Craiciu, A. Arbabi, T. Zhong, A. Faraon, Coupling erbium dopants in yttrium orthosilicate to silicon photonic resonators and waveguides. *Opt. Express* **25**, 2863–2871 (2017)
23. F.L. Kien, A. Rauschenbeutel, Nanofiber-mediated chiral radiative coupling between two atoms. *Phys. Rev. A* **95**, 023838 (2017)
24. P. Schneeweiss, S. Zeiger, T. Hoinkes, A. Rauschenbeutel, J. Volz, Fiber ring resonator with nanofiber section for chiral cavity quantum electrodynamics and multimode strong coupling. *Opt. Lett.* **42**, 85–88 (2017)
25. D.J. Alton, N.P. Stern, T. Aoki, H. Lee, E. Ostby, K.J. Vahala, H.J. Kimble, Strong interactions of single atoms and photons near a dielectric boundary. *Nat. Phys.* **7**, 1569–165 (2011)
26. A. Asenjo-Garcia, J.D. Hood, D.E. Chang, H.J. Kimble, Atom-light interactions in quasi-1d nanostructures: a green's function perspective". *Phys. Rev. A* **95**, 033818 (2017)
27. A.P. Burgers, L.S. Peng, J.A. Muniz, A.C. McClung, M.J. Martin, H.J. Kimble, Clocked atom delivery to a photonic crystal waveguide. *Proc. Nat. Acad. Sci. USA* **116**, 456–465 (2019)
28. J.S. Douglas, H. Habibian, C.-L. Hung, A.V. Gorshkov, H.J. Kimble, D.E. Chang, Quantum many-body models with cold atoms coupled to photonic crystals. *Nat. Photonics* **9**, 326–331 (2015)
29. A. Goban, C.-L. Hung, J.D. Hood, S.-P. Yu, J.A. Muniz, O. Painter, H.J. Kimble, Superradiance for atoms trapped along a photonic crystal waveguide. *Phys. Rev. Lett.* **115**, 063601 (2015)
30. J.D. Hood, A. Goban, A. Asenjo-Garcia, M. Lu, S.P. Yu, D.E. Chang, H.J. Kimble, Atom-atom interactions around the band edge of a photonic crystal waveguide. *Proc. Natl. Acad. Sci. USA* **113**, 10507 (2016)
31. J.P. Covey, A. Sipahigil, S. Szoke, N. Sinclair, M. Endres, O. Painter, Telecom-band quantum optics with ytterbium atoms and silicon nanophotonics. *Phys. Rev. Appl.* **11**, 034044 (2019)
32. U.P. Dharanipathy, M. Minkov, M. Tonin, V. Savona, R. Houdre, High-q silicon photonic crystal cavity for enhanced optical nonlinearities. *Appl. Phys. Lett.* **105**, 101101 (2014)
33. J. Zhanga, W. Liu, Y. Shi, S. He, High-q side-coupled semi-2d-photonic crystal cavity. *Sci. Rep.* **6**, 26038 (2016)
34. A.H. Safavi-Naeini, T.P.M. Alegre, M. Winger, O. Painter, Optomechanics in an ultrahigh-q two-dimensional photonic crystal cavity. *Appl. Phys. Lett.* **97**, 101106 (2010)
35. T.-H. Xiao, Z. Zhao, W. Zhou, M. Takenaka, H.K. Tsang, Z. Cheng, K. Goda, Mid-infrared germanium photonic crystal cavity. *Opt. Lett.* **42**, 2882 (2017)
36. S.X. Tao, A.M.M.G. Theulings, V. Prodanovic, J. Smedley, H.V. der Graaf, Optical properties of silicon-rich silicon nitride (sixnyhz) from first principle. *Computation* **3**, 657–669 (2015)
37. K. Srinivasan, M. Borselli, O. Painter, A. Stintz, S. Krishna, Cavity q, mode volume, and lasing threshold in small diameter algaas microdisks with embedded quantum dots. *Opt. Express* **14**, 1094 (2006)
38. P. Siddons, C.S. Adams, C. Ge, I.G. Hughes, Absolute absorption on rubidium d lines: comparison between theory and experiment. *J. Phys. B: At. Mol. Opt. Phys.* **41**, 1552004 (2008)
39. D. A. Steck, "Rubidium 87 d line data," tech. rep., Theoretical Division (T-8), Los Alamos National Laboratory, Los Alamos, NM 87545, (2001)
40. S. Scheel, S.Y. Buhmann, C. Clausen, P. Schneeweiss, Directional spontaneous emission and lateral casimir-polder force on an atom close to a nanofiber. *Phys. Rev. A* **92**, 043819 (2015)
41. S.Y. Buhmann, *Dispersion Forces I: Macroscopic Quantum Electrodynamics and Ground-State Casimir, Casimir Polder and van der Waals Forces*. (Springer, Berlin, 2012)
42. M. Meucci, E. Mariotti, P. Bicchi, C. Marinelli, L. Moi, Light-induced atom desorption. *Europhys. Lett.* **25**, 639 (1994)
43. C. Klempt, T. van Zoest, T. Henninger, O. Topic, E. Rasel, W. Ertmer, J. Arlt, Ultraviolet light-induced atom desorption for large

- rubidium and potassium magneto-optical traps. *Phys. Rev. A* **73**, 013410 (2006)
44. L. Torralbo-Campo, G.D. Bruce, G. Smirne, D. Cassettari, Light-induced atomic desorption in a compact system for ultracold atoms. *Sci. Rep.* **5**, 14729 (2015)
  45. D.S. Barker, E.B. Norrgard, J. Scherschligt, J.A. Fedchak, S. Eckel, Light-induced atomic desorption of lithium. *Phys. Rev. A* **98**, 043412 (2018)
  46. F. Ripka, H. Kübler, R. Löw, T. Pfau, A room-temperature single-photon source based on strongly interacting rydberg atoms. *Science* **362**, 446–449 (2018)
  47. N. Liu, L. Langguth, T. Weiss, J. Kastel, M. Fleischhauer, T. Pfau, H. Giessen, Plasmonic analogue of electromagnetically induced transparency at the drude damping limit. *Nat. Mater.* **8**, 758 (2009)
  48. X. Wu, S.K. Gray, M. Pelton, Quantum-dot-induced transparency in a nanoscale plasmonic resonator. *Opt. Express* **23**, 23633 (2010)
  49. Y.-H. Lien, G. Barontini, M. Scheucher, M. Mergenthaler, J. Goldwin, E.A. Hinds, Observing coherence effects in an overdamped quantum system. *Nat. Commun.* **7**, 13933 (2016)
  50. C. Li, X. Chai, B. Wei, J. Yang, A. Daruwalla, F. Ayazi, C. Raman, Cascaded collimator for atomic beams traveling in planar silicon devices. *Nat. Commun.* **10**, 1831 (2019)
  51. A.B. Khanikaev, G. Shvets, Two-dimensional topological photonics. *Nat. Photonics* **11**, 763 (2017)

**Publisher's Note** Springer Nature remains neutral with regard to jurisdictional claims in published maps and institutional affiliations.